Dalton Transactions

Accepted Manuscript

ROYAL SOCIETY OF CHEMISTRY

www.rsc.org/dalton

Isomeric Chain Structures of $\{[Mn(H_2O)_4]_2Ru_2(CO_3)_4Br_2\}_n^{n-}$: Syntheses, Structural Diversity and Magnetic Properties

Xiao-Feng Hou,[a] Yan-Yan Jia,[a] Jian-Hui Yang,[a] Zhi Cao,[b,*] Bin Liu,[a,*]

[a]*Key Laboratory of Synthetic and Natural Functional Molecule Chemistry of Ministry of Education, College of Chemistry & Materials Science, Shaanxi Key Laboratory of Physico-Inorganic Chemistry, Northwest University, Xi'an 710069, P. R. China*

[b]*Department of Chemistry, University of California, Berkeley, California 94720, United States*

Abstract

Self-assemblings of $Ru_2(CO_3)_4^{3-}$ paddle-wheel precursors and Mn^{2+} ions in aqueous solution yield various carbonate complexes. With appropriate selections of the synthetic conditions, we are able to intentionally tune the compositions and the structures of Mn-Ru_2-carbonato assemblies forming infinite chain structural complexes: $K[\{Mn(H_2O)_4\}_2Ru_2(CO_3)_4Br_2]\cdot H_2O$ (**1**) and $H[\{Mn(H_2O)_4\}_2Ru_2(CO_3)_4Br_2]\cdot 6H_2O$ (**2**). Complexes **1** and **2** are obtained at varied temperatures (25 ℃ for **1** and 5 ℃ for **2**, respectively), and their crystal structures consist of brick-wall stacked chains, in which neighboring $Ru_2(CO_3)_4Br_2^{5-}$ units are linked by two disubstituted octahedral $Mn(H_2O)_4^{2+}$ in a *cis* manner, resulting in two isomeric (twisted and zigzag) negative double-chain α- and β-$\{[Mn(H_2O)_4]_2Ru_2(CO_3)_4Br_2\}_n^{n-}$. Magnetism properties of complexes **1** and **2** are thoroughly characterized. The alternating current (AC) susceptibility analysis of complex **1** reveals a two-step magnetism transition at T_1 = 5.0 K and T_2 = 2.6 K, respectively. Complex **2** exhibits metamagnetism behavior with a transition field H_C = ~1.2 kOe at 2.0 K.

Keywords: Diruthenium · Manganese ·Carbonates · Chain structure · Magnetic properties

Introduction

* Corresponding author. Tel./fax: +86-029-88302604.

E-mail address: liubin@nwu.edu.cn (B. Liu); zcao@berkeley.edu (Z. Cao)

O,O'- and N,N'-donor ligands chelating and bridging metal-metal bonded diruthenium core have attracted broad interests in the field of molecular-based materials.[1] Such paddle-wheel units are of particular interest due to their important roles as building blocks for construction of wires, switches and other molecular devices.[2] Moreover, the higher Curie Temperatures (T_C) have been evident in both conducting and magnetism ordering metal coordination polymers with framework structures.[3] The featured high spin ground states for this type of dimers are due to both the near degeneracy of the π^* and δ^* orbitals,[4] and the unusually large zero-field splitting D.[5] Because of these facts, the heterometallic carboxylate M-Ru_2 systems based on mixed-valent $Ru_2(RCO_2)_4^+$ units exhibiting magnetism ordering have drawn considerable interests, since the discovery the first ferrimagnet $[Ru_2(MeCO_2)_4]_3[Cr(CN)_6]$ (T_c = 33 K), constructed from two independent lattice interpenetrating structure by the research group of Miller.[6a] Recently, some 2D and 3D magnets with $Ru_2(RCO_2)_4^+$ (R = H, Me, and Bu^t) bridged $[W(CN)_8]^{5-}$[3a] and $[M(CN)_6]^{3-}$ (M = Fe and Cr)[6] exhibiting high critical temperatures (T_c) have also been successfully prepared.

The prevalent non-carboxylate-type O,O'-donor bridging ligands used for the construction of Ru_2^{n+} paddlewheel building blocks are CO_3^{2-},[7] SO_4^{2-},[8] $H_nPO_4^{(3-n)-}$[9] and $H_nhedp^{(2-n)-}$(hedp = 1-hydroxyethylidenediphosphonate, $CH_3C(OH)(PO_3)_2$).[10] Among them, CO_3^{2-} ligand has been demonstrated efficiently in mediating the magnetic exchange interaction due to its unique features, such as multi-coordination number, versatile configurations, and more diffused axial and equatorial direction orbitals, and is thus a promising building block for molecular-based magnets. The initial attempts of these endeavors were the coordination of this paramagnetic unit with light transitional metal ions, forming three dimensional weak ferromagnets $K_xH_{1-x}[M(H_2O)_4][Ru_2(CO_3)_4]\cdot nH_2O$ (M = Mg, Mn, Fe, Co, Ni).[7a-c] Our efforts to design new molecular-based magnets have led to the development of 3d-4d heterometallic diruthenium carbonates, in which multidentate CO_3^{2-} ligands chelate and bridge Ru-Ru bonds core, preventing its further decomposition, and the remaining carbonate oxygen atoms are linked with 3d metal ions through varieties of manners (for instance, *cis*, *trans* and cross shape), resulting in different topology frameworks.[11] These heterometallic carbonates display interesting magnetic properties with strong ferromagnetic intramolecular spin-spin interactions, and are of ideal building blocks to

construct for low dimensional molecule-based magnets, such as SMMs and SCMs. In this contribution, we report the syntheses and characterizations of two novel chain structural carbonates $K[\{Mn(H_2O)_4\}_2Ru_2(CO_3)_4Br_2]\cdot H_2O$ (**1**) and $H[\{Mn(H_2O)_4\}_2Ru_2(CO_3)_4Br_2]\cdot 6H_2O$ (**2**). The structural diversity can be turned by selection of the appropriate condition of self-assembling reactions between two precursors $Ru_2(CO_3)_4^{3-}$ and Mn^{2+}. Although studies of carboxylate chain complexes $[\{Ru_2(piv)_4\}_3W(CN)_8(H_2O)]$, $(PPh_4)_2[Ru_2(piv)_4W(CN)_8]\cdot 0.5H_2O$ (Hpiv = pivalic acid)[3a] and $Na_7[Ru_2(hedp)_2Fe(CN)_6]\cdot 24H_2O$[10b] had been documented previously, to our best knowledge, the heterometallic chain structural complexes based on $Ru_2(CO_3)_4^{3-}$ motif have never been explored yet.

Experimental Section

Materials and Physical Measurements

$K_3[Ru_2(CO_3)_4]\cdot 4H_2O$ is prepared according to the method described previously.[7e] All reagents were used as received without further purification. Elemental analyses are performed on a Perkin-Elmer 2400 CHN elemental analyzer. The composition of K, Mn and Ru is analyzed on an IRIS Advantage ICP atomic emission spectrometer. Infrared spectra are recorded in the range of 400–4000 cm^{-1} on an EQUINOX55 FT/IR spectrophotometer using KBr pellets. TGA curves are recorded on Netzsch STA 449C microanalyzer under N_2 atmosphere at a heating rate of 10 °C·min^{-1}. The X-ray powder diffraction (XRPD) data are recorded on a Rigaku RU200 diffractometer at 60 KV, 300 mA and Cu Kα radiation (λ = 1.5406 Å), with a scan rate of 5°/min and a step size of 0.02° in 2θ. Magnetic measurement results are obtained on polycrystalline samples (4.33 mg for **1** and 5.11 mg for **2**) by using a Quantum Design MPMS-XL7 SQUID magnetometer at temperatures between 1.8 and 300 K for direct current (dc) applied fields (restrained in eicosane to prevent torqueing at high fields). Alternating current (AC) susceptibility measurements for all complexes are performed by using an AC field of 3.5 Oe, with frequencies ranging from 1 to 1000 Hz. All experimental susceptibilities are corrected for the diamagnetism of the constituent atoms (Pascal's constants).[12]

Synthesis of $K[\{Mn(H_2O)_4\}_2Ru_2(CO_3)_4Br_2]\cdot H_2O$ (**1**)

$K_3[Ru_2(CO_3)_4]_3\cdot 4H_2O$ (0.05g, 0.079 mmol) and $LiBr\cdot H_2O$ (0.500 g, 4.76 mmol) are dissolved in

15 mL H_2O. To this solution, $Mn(CH_3CO_2)_2 \cdot 4H_2O$ (0.081 g, 0.33 mmol) in 5 mL H_2O is added with 30 minutes stirring at room temperature. Dark-brown square block crystals are obtained upon standing after a month, with a yield of 21% (based on Ru). Anal. Calcd for $C_4H_{18}KMn_2Br_2Ru_2O_{21}$: C, 5.26; H, 1.99; K, 4.28; Mn, 12.03; Ru, 22.14. Found C, 5.10; H, 2.00; K, 4.30; Mn, 11.60; Ru, 21.60. **IR** (**KBr**, υ/cm^{-1}) for **1**: 3427(br, vs), 1628(m), 1499(vs), 1391(w), 1281(m), 1065(w), 815(w), 713(br, m), 416(w).

Synthesis of $H[\{Mn(H_2O)_4\}_2Ru_2(CO_3)_4Br_2] \cdot 6H_2O$ (**2**)

The synthetic procedure for **2** is similar to that of **1** except for decreasing the reaction temperature to 15℃. The mixture is kept at 5℃ for an extended period of time (greater than 2 weeks), dark-brown column crystals of **2** are isolated (yield: 0.033 g, 44%, based on Ru). Anal. Calcd for $C_4H_{29}Mn_2Br_2Ru_2O_{26}$: C, 4.98; H, 3.03; Mn, 11.39; Ru, 20.95. Found C, 4.80; H, 3.20; Mn, 11.50; Ru, 21.00. **IR** (**KBr**, υ/cm^{-1}) for **2**: 3448(br, vs), 1634(s), 1510(s), 1283(m), 1100(w), 1068(w), 814(w), 621(br, m).

Single-crystal X-ray diffraction. Single-crystal diffraction data for complexes **1** and **2** are collected on Rigaku SCX mini CCD diffractometer by using a graphite-monochromatized Mo Kα radiation (λ = 0.71073 Å) at room temperature. The data integration and reduction are processed with SAINT software. Absorption correction based on multi-scan is performed based on SADABS program. The structures are solved by the direct method using SHELXTL and refined by a full-matrix least-squares method on F^2 with SHELXL-97 program.[13] All non-hydrogen atoms are refined anisotropically. Crystallographic data, selected bond lengths and angles with their estimated standard deviations of the complexes are shown in **Table 1**, **Table 2** and **Table S1** (Supplementary information).

Table 1 **Table 2**

Results and Discussion

Synthesis

Complexes **1** and **2** are prepared through the self-assembling of $Ru_2(CO_3)_4^{3-}$ precursors and

Mn^{2+} ions in aqueous solution. The synthetic routes of self-assembling of $Ru_2(CO_3)_4^{3-}$ and Mn^{2+} in aqueous solution are shown in scheme **1**. For the well-known self-assembling reactions, a number of associated factors may influence the afforded products, for instance, the reaction temperature, molar ratio of the starting materials, presence of templates, pH, chosen reaction medium, etc. Our initial attempts to grow large crystals of the series of 3D network complexes $K_xH_{1-x}[M(H_2O)_4][Ru_2(CO_3)_4]\cdot nH_2O$ (M = Mg, Mn, Fe, Co, Ni), synthesized by Miller's group through a syringe pump method, are not straightforward. However, a complex of $K[Mn(H_2O)_5Ru_2(CO_3)_4]\cdot 5H_2O$ with desired 2D layered structure, has been successfully prepared.[11g] This prompted us to perform a systematic investigation of the self-assembling conditions toward desired targets. The reaction of $Ru_2(CO_3)_4^{3-}$ with excess of Mn^{2+} (the molar ratio of Ru_2/Mn is 1/4) in an aqueous solution at 20 ℃ gives a novel 3D framework complex $Mn_4(H_2O)_{16}H[Ru_2(CO_3)_4]_2[Ru_2(CO_3)_4(H_2O)_2]\cdot 11H_2O$, with a magnetic ordering below 3.5 K.[11a] Moreover, we have also explored the self-assembling of $Ru_2(CO_3)_4^{3-}$ and Mn^{2+} in the presence of Cl^- and have obtained a layered structural complex $KMn(H_2O)_6[Mn(H_2O)_2Ru_2(CO_3)_4Cl_2]\cdot 4H_2O$.[11d] In this work, upon careful selection of reaction conditions for the self-assembling between $Ru_2(CO_3)_4^{3-}$ and Mn^{2+}, two novel chain structural complexes **1** and **2** have been synthesized. It turns out that the existence of both $CH_3CO_2^-$ and excess of Br^- is the key component to secure the crystal quality of complex **1** and **2**. Attempts to use $MnCl_2$, $Mn(NO_3)_2$, $MnSO_4$ and $Mn(ClO_4)_2$ in the synthetic procedure fail to form pure phases of complexes **1** and **2**, as evident in the $Mn(CH_3CO_2)_2$ case. This may attribute to the existence of carboxylic acid ligands, in which $CH_3CO_2^-$ maintains the aqueous solution in an appropriate pH condition. Further replacement of Br^- by Cl^- in the preparation of complex **1** and **2** has also been proved unsuccessful.

Scheme. 1

Crystal Structures

*$K[\{Mn(H_2O)_4\}_2Ru_2(CO_3)_4Br_2]\cdot H_2O$ (**1**).* Single-crystal X-ray diffraction studies reveal that complex **1** is crystallized in a tetragonal space group of $P4_2/mbc$. As shown in **Fig 1. Top**, the ORTEP plot consists of a crystallographically independent quarter of $[Ru_2(CO_3)_4Br_2]^{5-}$ dimer, half of $Mn(H_2O)_4^{2+}$, and disordered K^+ and water O6 per asymmetric unit. For the paddlewheel dimer,

the axial positions of $Ru_2(CO_3)_4^{3-}$ unit are occupied by Br^- ions. The Ru(1)–Ru(1A) [2.2780(13) Å] and the Ru–O bond lengths [2.029(5)–2.035(5) Å] in **1** are comparable to those related complexes.[7,11] The Ru(1)–Br(1) bond distance [2.7234(16) Å] is in agreement with that found in $[\{Co(H_2O)_4\}_2Ru_2(CO_3)_4(H_2O)_2]\cdot[\{Co(H_2O)_4\}_2Ru_2(CO_3)_4Br_2]\cdot 10.5H_2O$ [2.517–2.587 Å].[11c] The Mn^{2+} ion is six-coordinated in a distorted octahedron $MnOc_2Ow_4$, where Oc represents carbonate and Ow water oxygen atoms, and Mn-O bond lengths fall in the range of 2.170(5) to 2.240(6) Å. The O–Mn(1)–O angles have been evidently deviated from 90° and varied from 77.4(3)° to 100.0(2)°. Herein, two CO_3^{2-} groups of the neighboring paddle-wheel Ru_2 dimers are linked via two Mn^{2+} bridges in a *cis* mode, with the angle 129.7(5)° of C(1)–O(3)–Mn(1) in the bridging pathway, yielding an infinite double-twisted chain structure, α-$\{[Mn(H_2O)_4]_2Ru_2(CO_3)_4Br_2\}_n^{n-}$, running along the *c* direction (Fig. 1 Middle). The shortest intrachain Mn(1)···Ru(1) (1 - x, 2 - y, z) and Mn(1)···Mn(1) (1 - x, 2 - y, z) distances are 5.371(1) and 7.786(2) Å, respectively. The low symmetry of this chain structure precludes an easy localization of this Jahn–Teller axis with respect to the crystallographic axis. The hydrogen bonds arising from the carbonate oxygen atoms and the coordination water molecules of the octahedron MnO_6 bridges help keeping the chains tightness with a novel brick-wall packing diagram.(Fig. 1 Bottom) The hydrogen bonds are mainly formed between O(1) and O(4) (x, 1 - y, 0.5 - z), O(2) and O(4) (3/2 - y,3/2 - x,1/2 - z), O(3) and O(5) (0.5 + x, 1.5 - y, z). The O(1)···O(4), O(2)···O(4) and O(3)···O(5) distances are 2.772(8), 2.705(8) and 2.763(8) Å, respectively. The shortest interchain Ru···Mn and Mn···Mn distances are 5.338(1) and 5.969(2) Å, respectively, much shorter than that of the shortest interchain Ru· · ·Ru distance [7.070(2) Å]. Disordered K^+ and water molecules sitting in the void space, and the K–O or hydrogen bonds O(6)···O distances fall in the range of 2.901(6) – 3.116(7) Å.

Figure. 1

*$H[\{Mn(H_2O)_4\}_2Ru_2(CO_3)_4Br_2]\cdot 6H_2O$ (**2**)*. Noticing that the temperature might play an important role in directing the self-assembling of products with diverse structural topologies,[11b,f] we changed the experimental conditions to a lower temperature 5 ℃. Fortunately, we obtained the 1D structural complex **2**, which is constructed of an interesting double-zigzag chain

β-{[$Mn(H_2O)_4$]$_2$$Ru_2(CO_3)_4Br_2$}$_n^{n-}$. Complex **2** is crystallized in the monoclinic space group of *C*/2*m*. As shown in Fig 2. Top, there are two crystallographically independent quarter of Ru1Ru1A and Ru2Ru2B dimers, which are linked by one crystallographically independent octahedral environment Mn1 and its equivalent Mn1C in a *cis* fashion forming the isomeric double-chain structure (Fig 2. Middle). The Ru(1)–Ru(1A) [2.2693(13) Å], Ru(2)–Ru(2B) [2.2731(10) Å], Ru(1)–Br(1) [2.7267(17) Å] and Ru(2)–Br(2) [2.6948(13) Å] are in agreement with those in complex **1**. The Ru–O bond lengths [2.015(5)–2.027(5) Å] in **2** are comparable to those in **1** and the related complexes.[7,11] Mn-O bond lengths fall in the range of 2.146(6) to 2.203(5) Å, and the O–Mn(1)–O angles vary from 87.4(3)° to 94.3(2)°, which demonstrate a weaker distortion of Mn in **1** than in **2**. The angles C(1)–O(2)–Mn(1) and C(2)–O(5)–Mn(1) are 131.2(5) and 128.8(4)°, respectively. The shortest intrachain distances Mn(1)···Ru(1), Mn(1)···Ru(2) and Mn(1)···Mn(1) are 5.312(1), 5.386(1) and 7.643(2) Å, respectively. The two isomeric chains, the twisted α- and double-zigzag chain β-{[$Mn(H_2O)_4$]$_2$$Ru_2(CO_3)_4Br_2$}$_n^{n-}$, are compared in Fig 3. Different from that in complex **1**, none K atoms have been found for the single crystal analysis of **2**, which is in agreement with the elemental analysis results. The hydrogen bonds keep these zigzag chains tightness with a new parallel brick-wall packing diagram.(Fig. 2 Bottom). The shortest interchain Ru···Mn and Mn···Mn distances are 6.395(2) and 5.471(2) Å, respectively, also shorter than that of the shortest interchain Ru···Ru distance [8.724(1) Å].

Figure. 2

Figure. 3

IR, PXRD and TG Results

In the IR spectra of complexes **1** and **2** (Figs S1 and S2, ESI), the presence of the broad and strong characteristic stretching frequency in the region of 3200−3700 cm^{-1} are assigned to the characteristic peaks of OH vibration of lattice water. A series of intense bands between 1550 and 700 cm^{-1} correspond to the fundamental or splitting vibration of the carbonate groups CO_3^{2-}.[14]

In order to confirm the phase purity of the bulk materials used for magnetism measurements, X-ray powder diffraction (XRPD) experiments have been performed for complexes **1** and **2**, and the experimental and simulated patterns are shown in Figs S3−S4, respectively. Clearly, the experimental patterns of **1** and **2** are in good agreement with the prediction of simulations,

indicating the phase purity of the as-synthesized products.

Thermal analysis of complex **1**(Fig. S5, ESI) reflects a mass loss (19.49%) in the temperature range of 30—250 ℃, lower than the value of removal of one lattice water and eight coordinated water molecules (Calcd. 17.74%), and this may be attributed to the residual solvents on the surface of samples. Continuous heating the samples above 250 ℃ would result in a faster mass loss in the temperature range of 250—315 ℃, likely due to the decomposition of the main structure. The mass loss of 19.40% is in agreement with the release of four CO_2 (Cal. 19.28%).

The thermal behavior of **2** bears extensive similarity as that of **1**. As shown in Fig S6, a mass loss 26.05% in the temperature of 30—250 ℃ for complex **2** is attributed to the removal of six lattice water and eight coordinated water molecules (Calcd. 26.13%). Heating over 320 ℃, the main structure decomposes, and a faster mass loss (19.82%) in the temperature range of 250—320 ℃ is consistent with the release of four CO_2 (Calcd. 18.24%). Above 320 ℃, the continuous mass loss is probably associated to a slow release of HBr.

Magnetic Properties

The magnetic properties of complex **1** in the form of $\chi_M T$ versus T plot are shown in Fig 4. At room temperature, $\chi_M T$ is 10.95 cm^3 K mol^{-1}, which is higher than the spin-only value of 10.63 cm^3 K mol^{-1} expected for one Ru_2 dimer (g = 2, S = 3/2) and two Mn^{2+} (g = 2, S = 5/2), due to the presence of zero-field splitting primarily arising from the $Ru_2^{II,III}$.[5] Upon cooling, $\chi_M T$ starts to slowly increase till to 25 K. Subsequently, it increases drastically and reaches to a value of 29.18 cm^3 K mol^{-1} at 3.0 K, followed by a drop to 24.80 cm^3 K mol^{-1} at 1.8 K. Typically, arising from mixed-valent Ru_2 core, the positive zero-field splitting D would result in the $\chi_M T$ deceasing upon cooling in the high temperature range. Herein, the monotonous increase cooling in the temperature range 300 – 20 K is attributed to the strong ferromagnetic exchange between the paramagnetic centers Ru_2 and Mn through the μ_3-CO_3^{2-} bridges, which has been well-established in the 3D structure complex $Mn_4(H_2O)_{16}H[Ru_2(CO_3)_4]_2[Ru_2(CO_3)_4(H_2O)_2]\cdot 11H_2O$.[11a] The abrupt increase in $\chi_M T$ suggests the onset of magnetic ordering, and the subsequent decrease of $\chi_M T$ below 3.0 K is the result of a saturation of the χ_M value and/or the zero-field splitting effect. Based on Equation 1, a least-squares fitting procedure is applied (with fixed g_{Mn} = 2), and the fitting pattern above 25 K, as represented in solid line in Fig 4 offers the parameters: g_{Ru} = 2.13, D = 90.2 cm^{-1}, θ = 3.82 K

and $R = 4.3 \times 10^{-4}$ (the error factor R is defined as $\sum[(\chi_M T)_{obsd} - (\chi_M T)_{calcd}]^2 / \sum[(\chi_M T)^2_{obsd}]$). The positive Weiss constant θ value, roughly accounts for the intrachain interactions, demonstrates the ferromagnetic coupling between Ru_2 dimer and Mn through CO_3^{2-} bridges.

Figure. 4 **Figure. 5**

$\chi = \chi_{Ru_2} + 2\chi_{Mn}$,

where $$\chi_{Ru_2} = \frac{Ng_{Ru}^2\beta^2}{k(T-\theta)}\left[\frac{1}{3}\frac{1+9e^{-2D/kT}}{4(1+e^{-2D/kT})} + \frac{2}{3}\frac{1+(3kT/4D)(1-e^{-2D/kT})}{1+e^{-2D/kT}}\right] \quad (1)$$

and $$\chi_{Mn} = \frac{Ng_{Mn}^2\beta^2}{3k(T-\theta)}S(S+1)$$

As shown in the inset of Fig 4, the χ_M vs T curve recorded at 0.5 kOe features a peak around 2.4 K, corresponding to an antiferromagnetic (AF) ordering at a low field. When the external field is increased, the peak in the χ_M vs. T curve becomes broader and completely disappears above 2.0 kOe. The transition to an AF state can be directly reflected by the in phase of zero-field alternating current (AC) magnetic susceptibility χ_M'(Fig 5), which features a broad peak coexistence with a small sharp peak at *ca*. 2.6 K under H_{ac} = 3.5 Oe with frequencies of 1, 10, 100 and 1000 Hz. The small and sharp signal at same temperature has been observed for χ_M". However, no frequency dependence of χ_M" on both in-phase and out-of-phase signals is observed, reflecting a magnetic ordering occurring below 2.6 K. Since lack of a signal in the imaginary part of the AC susceptibility in antiferromagnets, the weak ferromagnetic behavior of complex **1** is likely derived from the perpendicular brick-wall alignment of these ferromagnetic chain $\{[Mn(H_2O)_4]_2Ru_2(CO_3)_4Br_2\}_n^{n-}$. The same phenomenon has been witnessed in the β polymorph of Mn^{2+} phthalocyanine, in which the stacking of two types of ferromagnetic chains of MnPc forms an angle of *ca*. 90° between two adjacent neighbors.[15] Increasing temperature up to 5.0 K, the second magnetic ordering occurs, and two more peaks at 4.9 K in χ' and around 4.6 K in χ" with respect to the AC susceptibility appear. The signal positions of both the in-phase (χ') and out-of-phase (χ'') shift to higher values with increasing frequency. The shift of the peak temperature (T_p) of χ" can be quantified by $\phi = (\mathrm{V}T_P / T_P)/\mathrm{V}(\log f) = 0.016$, while the obtained

f values are 0.016, which are typical for normal spin glasses.[16] The frequency dependence of T_p on χ_M" can be expressed by Arrhenius equation, $\tau = \tau_0 \exp(VE / k_B T)$ (τ is the relaxation time, τ_0 is the pre-exponential factor, and ΔE is the energy gap; Fig S7), giving parameters of $\tau_0 = 2 \times 10^{-75}$ s and $\Delta E/k_B = 774(6)$ K. Such large parameter values reveal that the magnetic relaxation behavior around 4.9 K is mainly attributed to the spin-glass-like dynamic process. Similar glass behavior for a series of oxalate-based bimetallic frameworks $\{M^{II}Cr^{III}(ox)_3\}_n^{n-}$ (Mn^{II} = Mn, Fe, Co and Ni) has also been reported by Coronado and co-workers.[17]

Figure. 6

For a better understanding of the two AC susceptibility peaks associated with the two steps of magnetic ordering transitions, we have performed measurements of field-cooling (FC) and zero-field-cooling (ZFC), with FC-ZFC curves provided in Fig 6. The ZFC and FC plots are measured with an external field of 10 Oe. The ZFC measurement protocol is performed as follows: first, the sample is cooled to the lowest temperature (T = 1.8 K) at zero field; then, the measuring magnetic field is applied and the magnetization recorded as the sample's temperature has been increased at a constant sweep rate of about 0.5 K/min. The only difference in the protocol of FC and ZFC is that in the former case, the measuring applied field has been applied before cooling the sample. The ZFC magnetization increases from an initial value at T = 1.8 K to a maximum at 2.6 K; then it starts to drop till to 3.5 K. Upon heating, it begins to increase again until reaching a second maximum at 4.8 K, above which it decreases until room temperature. Consistent with the ZFC plot, the FC increases upon cooling, deviates from the ZFC at 5.0 K, and then reaches a maximum at 2.3 K. A similar behavior has been observed for the layer structural metamagnet $[\{Co(H_2O)_4\}_2Ru_2(CO_3)_4(H_2O)Cl]_n \cdot 7.5nH_2O$, which generates a FC-ZFC deviation at 5.0 K (Cuie ordering below 5.1 K proved by ac susceptibilities measurements), with a maximum at around 2.6 K (Antiferromagnetic ordering occurs below this temperature).[11c] Both AC and FC-ZFC measurements reveal a two-step magnetic phase transitions in the temperature range 1.8–8.0 K. The first step occurs at *ca.* 2.6 K, and the signals appear from both χ' and χ", which are typical for a metamagnetic transition from an antiferromagnetic state to a ferromagnetic state coexistence of magnetic ordering possibly due to the structure transition occurring at this temperature position.

Two steps magnetic ordering was also found in a molecular-based magnet with a formula of $[CrCyclam(CtC\text{-}Ph)_2][Ni(mdt)_2](H_2O)$ (Cyclam = 1,4,8,11-tetraazacyclotetradecane, mdt = 1,3-dithiole-4,5-dithiolate), and the transitions occur at 2.9 and 3.7 K, respectively.[18] As our best knowledge, to date, the reported heterometallic complexes with two-step magnetic ordering behavior are very rare.

Figure. 7

The field-dependent magnetization of complex **1** was tested up to 50 kOe at 2.0 K. As shown in Fig 7, the magnetization increases rapidly with the increasing field below 4 kOe, and then keep increasing but slowly, until reaching its highest value about 11.6 Nβ at 50 kOe, consistent with the spin-only value for magnetically isolated two Mn^{2+} ions and one $Ru_2^{II,III}$ dimmer. The hysteresis loop in the field range of -0.5—0.5 kOe represents a sigmoid behavior with a coercive field of *ca*. 0.04 kOe and remnant magnetization of *ca*. 0.087 N*β*.

Figure. 8

For complex **2** (as shown in Fig 8), the $\chi_M T$ versus T curve exhibits a similar behavior with complex **1**. The $\chi_M T$ value at room temperature is 11.19 cm^3 K mol^{-1}, and upon cooling, $\chi_M T$ slowly increases till to 25 K. Subsequently, it increases drastically and reaches a value of 32.97 cm^3 K mol^{-1} at 3.0 K, followed by a drop to 19.86 cm^3 K mol^{-1} at 1.8 K. The susceptibility data above 25 K are fitted by the same equation used for complex **1**, and the best fit gives the parameters: $g_{Ru} = 2.20$, $D = 90.7$ cm^{-1}, $\theta = 4.78$ K and $R = 1.3 \times 10^{-3}$.

The χ_M vs T curves measured at 0.6, 1.0, 1.2, 1.4 and 2.0 kOe are shown in Fig 8 inset, in which the former four curves all feature a peak at *ca*. 2.5 K, implying a long-range antiferromagnetic (AF) ordering below this point, due to the AF interaction between the zigzag double chains. When the field is higher than 2.0 kOe, the peak in the plot of χ_M vs. T disappears, suggesting the occurrence of field-induced magnetic transitions. In Fig S8, the zero-field AC susceptibilities are measured and recorded in the range 2.0-6 K under $H_{ac} = 3.5$ Oe and frequencies of 1, 10 and 100 Hz. The AF transition is further evidenced by the in-phase susceptibilities $\chi_{M'}$, which has a peak at *ca.* 2.6 K (T_N), however, no detected out-of-phase signal and frequency dependence are observed near this temperature. Hence, the appearance of two phase transition points in complex **1**

undoubtedly excludes the possibility of the presence of composite of two complexes **1** and **2**.

Figure. 9

The intrachain ferromagnetic interaction is further evidenced by the saturation magnetization value of 13.0 Nβ (measured at 2.0 K and 50 kOe) (Fig 9), which is in good agreement with the spin-only value for magnetically isolated two Mn^{2+} ions and one Ru_2 dimer.[19] This saturation magnetization value is obviously larger than that (11.6 Nβ) of complex **1**, indicating the occurrence of a spin-canting in **1**. The magnetization of **2** reveals a sigmoid behavior (Fig S9), which first slowly increases with the increasing field and then follows a sharp spin-flipping from an antiferromagnetic arrangement to a ferromagnetic arrangement between the ferromagnetic chains. The critical field (Fig 9. inset), determined by the dM/dH curve, is *ca*. 1.2 kOe at 2.0 K. The important magnetic parameters for these heterometallic Mn-Ru_2 carbonates are summarized in Table 3.

Table. 3

Conclusions

In this contribution, we report the influence of reaction conditions on the self-assembling of $Ru_2(CO_3)_4^{3-}$ and Mn^{2+} ions in aqueous solution, resulting in two novel infinite chain structural complexes $K[\{Mn(H_2O)_4\}_2Ru_2(CO_3)_4Br_2]\cdot H_2O$ (**1**) and $H[\{Mn(H_2O)_4\}_2Ru_2(CO_3)_4Br_2]\cdot 6H_2O$ (**2**). Both of them follow a linear chain shape, in which the paddle-wheel $[Ru_2(CO_3)_4Br_2]^{3-}$ dimers are linked by the octahedral environment $Mn(H_2O)_4^{2+}$ in a *cis* manner, forming two isomeric α-(twisted) and β-(zigzag) chains $\{[Mn(H_2O)_4]_2Ru_2(CO_3)_4Br_2\}_n^{n-}$. However, those two chains exhibit different parallel brick-wall packing patterns. Ferromagnetic coupling has been evident between Ru_2 dimer and Mn though carbonate bridges. Complex **1** experiences two step magnetic ordering with T_1 = 5.0 K and T_2 = 2.6 K, respectively. While complex **2** has been proved to exhibit a metamagnetism behavior at T_N = 2.8 K, and the transition field (H_C) is ~1.2 kOe at 2.0 K. In this paper, we demonstrate the fact that varieties of possible factors relevant to the self-assembling reactions would have an impact on the formation of varied dimensions and structures of the target complexes. We anticipate that through an appropriately systematic and strategic tuning for the model complexes, it might be able to chase more fascinating magnetic properties.

Electronic supplementary information (ESI). Tables of selected bond angles of complexes and additional figures, IR, XRPD and TG graphs. CCDC 981894 and 981895 for **1** and **2**. For ESI and crystallographic data in CIF or other electronic format see DOI: 10.1039/c3dtxxxxxx.

Corresponding Author

Tel./Fax: +86 29 88302604. E-mail address: liubin@nwu.edu.cn (B. Liu.); zcao@berkeley.edu (Z. Cao)

Notes

The authors declare no competing financial interest.

Acknowledgments

This work was financially supported by the National Natural Science Foundation of China (No. 21101126), and the Education Commission of Shaanxi Province (No. 12JK0613).

References

1 (a) W. Kosaka, K. Yamagishi, A. Hori, H. Sato, R. Matsuda, S. Kitagawa, M. Takata and H. Miyasaka. *J. Am. Chem. Soc.* 2013, **135**, 18469; (b) M. Nishio, N. Hoshino, W. Kosaka, T. Akutagawa and H. Miyasaka. *J. Am. Chem. Soc.* 2013, **135**, 17715; (c) H. Miyasaka, T. Morita and M. Yamashita. *Chem. Commun*. 2011, **47**, 271; (d) H. Miyasaka, N. Motokawa, T. Chiyo, M. Takemura, M.o Yamashita, H. Sagayama and T. Arima. *J. Am. Chem. Soc.* 2011, **133**, 5338; (e) B. Xi, I. P.-C. Liu, G.-L. Xu, M. M. R. Choudhuri, M. C. DeRosa, R. J. Crutchley and T. Ren. *J. Am. Chem. Soc.* 2011, **133**, 15094; (f) J.-W. Ying, I. P-C. Liu, B. Xi, Y. Song, C. Campana, J.-L. Zuo and T. Ren. *Angew. Chem. Int. Ed*. 2010, **49**, 954.

2. M. C. Barral, S. Herrero, R. J. Aparicio, M. R. Torres and F. A. Urbanos. *Angew. Chem. Int. Ed.* 2005, **44**, 305.

3. (a) M. Mikuriya, D. Yoshioka, A. Borta, D. Luneau, D. Matoga, J. Szklarzewicz and M. Handa. *New. J. Chem*. 2011, **35**, 1226; (b) N. Motokawa, S. Matsunaga, S. Takaishi, H. Miyasaka, M. Yamashita and K. R. Dunbar. *J. Am. Chem. Soc.* 2010, **132**, 11943; (c) H. Miyasaka, N. Motokawa, S. Matsunaga, M. Yamashita, K. Sugimoto, T. Mori, N. Toyota and K. R. Dunbar. *J. Am. Chem. Soc.* 2010, **132**, 1532; (d) N. Motokawa, H. Miyasaka, M. Yamashita and K. R. Dunbar. *Angew. Chem. Int. Ed*. 2008, **47**, 7760.

4. (a) J. G. Jr. Norman, G. E. Renzoni and D. A. Case. *J. Am. Chem. Soc.* 1979, **101**, 5256; (b) G. Estiú, F. D. Cukiernik, P. Maldivi and O. Poizat. *Inorg. Chem.* 1999, **38**, 3030.

5. (a) F. A. Cotton, C. A. Murillo and R. A. Walton. Multiple Bonds Between Metal Atoms, 3rd ed., Springer Science and Business Media, New York, 2005; (b) M. Mikuriya.; D. Yoshioka and M.

Handa. *Coord. Chem. Rev.* 2006, **250**, 2194; (c) M. A. S. Aquino. *Coord. Chem. Rev.* 2004, **248**, 1025; (d) M. A. S. Aquino. *Coord. Chem. Rev.* 1998, **170**, 141.

6. (a) J. S. Miller. *Chem. Soc. Rev.*, 2011, **40**, 3266; (b) T. E. Vos and J. S. Miller. *Angew. Chem., Int. Ed.* 2005, **44**, 2416; (c) J. S. Miller, T. E. Vos and W. W. Shum. *Adv. Mater.* 2005, **17**, 2251; (d) B. S. Kennon, K. H. Stone, P. W. Stephens and J. S. Miller. *CrystEngComm.* 2009, **11**, 2185; (e) T. E. Vos, Y. Liao, W. W. Shum, J.-H. Her, P. W. Stephens,W. M. Reiff and J. S. Miller. *J. Am. Chem. Soc.* 2004, **126**, 11630; (f) Y. Liao, W. W. Shum and J. S. Miller. *J. Am. Chem. Soc.* 2002,**124**, 9336.

7 (a) B. S. Kennon and J. S. Miller. *Inorg.Chem.* 2010, 49, 5542; (b) B. S. Kennon, J.-H. Her, P. W. Stephens and J. S. Miller. *Inorg. Chem.* 2009, **48**, 6117; (c) B. S. Kennon, J.-H. Her, P. W. Stephens, W. W. Shum and J. S. Miller. *Inorg.Chem.* 2007, **46**, 9033; (d) J.-H. Her, B. S. Kennon, W. W. Shum, P. W. Stephens and J. S. Miller. *Inorg. Chim. Acta* 2008, **361**, 3462; (e) F. A. Cotton, L. Labella and M. Shang. *Inorg.Chem.*1992, 31, 2385; (f) A. J. Linday, G. Wilkinson, M. Motevalli and M. B. Hursthouse. *J. Chem. Soc. Dalton Trans.* 1987, *11*, 2723.

8 (a) A. N. Zhilyaev, T. A. Fomina, I. V. Kuzmenko, A. V. Rotov and I. B. Baranovskii. *Russ. J. Inorg. Chem.* 1989, **34**, 532; (b) I. V. Kuzmenko, A. N. Zhilyaev, T. A. Fomina, M. A. Porai-Koshits and I. B. Baranovskii. *Russ. J. Inorg. Chem.* 1989, **34**, 1457.

9 F. A. Cotton, T. Datta, L. Labella and M. Shang. *Inorg. Chim. Acta.* 1993, **203**, 55.

10 (a) X.-Y. Yi, L.-M. Zheng, W. Xu and S.-H. Feng. *Inorg. Chem.* 2003, **42**, 2827; (b) B. Liu, Y.-Z. Li and L.-M. Zheng. *Inorg. Chem.* 2005, **44**, 6921; (c) X.-Y. Yi, B. Liu, R. Jiménez-Aparicio, F. A. Urbanos, S. Gao, W. Xu, J.-S. Chen, Y. Song and L.-M. Zheng. *Inorg. Chem.* 2005, **44**, 4309; (d) B. Liu, P. Yin, X.-Y. Yi, S. Gao and L.-M. Zheng. *Inorg. Chem.* 2006, **45**, 4205; (e) B. Liu, B.-L. Li, Y.-Z. Li, Y. Chen, S.-S. Bao and L.-M. Zheng. *Inorg. Chem.* 2007, **46**, 8524; (f) B. Liu, T. Ding, W.-J. Hua, X.-M. Liu, H.-M. Hu, S.-H. Li and L.-M. Zheng. *Dalton Trans.*, 2013, **42**, 3429.

11. (a) B. Liu, J. Jin, X.-M. Liu, H.-M. Hu, T. Ding, N. Zhang, Y.-Y. Jia and G.-L. Xue. *Dalton Trans.,* 2012, **41**, 4748; (b) B. Liu, Y.-Y. Jia, J. Jin, X.-M. Liu, D. Wang and G.-L. Xue. *Dalton Trans.,* 2013, **42**, 10208; (c) B. Liu, Y.-Y. Jia, J. Jin, X.-M. Liu and G.-L. Xue. *CrystEngComm* 2013, **15**, 4280; (d) B. Liu, Y.-Y. Jia, H.-Q. Yang, J.-H. Yang and G.-L. Xue. *Dalton Trans*., 2013, **42**, 16742; (e) Y.-Y. Jia, B. Liu, X.-M. Liu and J.-H. Yang. *CrystEngComm* 2013, **15**, 7936; (f) B. Liu, D. Wang, J. Jin, Y.-Y. Jia, X.-M. Liu and G.-L. Xue. *CrystEngComm* 2013, 15, 5726; (g) Dan. Wang, B. Liu, J. Jin, X.-M. Liu, Y.-Y. Jia and G.-L. Xue. *Inorg. Chem. Commun.* 2013, **33**, 138.

12 (a) G. A. Bain and J. F. Berry. *J. Chem. Educ.* 2004, **85**, 532; (b) O. Kahn, Molecular Magnetism; VCH Publishers: New York, 1993.

13 (a) G. M. Sheldrick, SHELXL-97; University of Göttingen: Göttingen, Germany, 1997; (b) G.

M. Sheldrick, SADABS 2.05; University of Göttingen: Göttingen, Germany, 2002.

14 (a) K. Nakamoto, J. Fujita, S. Tanaka and M. Kobayashi. *J. Am. Chem. Soc.* 1957, **79**, 4904; (b) J. P. Jolivet, Y. Thomas and B. Taravel. *J. Mol. Struct.* 1982, **79**, 403.

15 S. Mitra, A. K. Gregson, W. E. Hatfield and R. R. Weller. *Inorg. Chem.* 1983, **22**, 1729.

16 J. A. Mydosh, Spin Glasses: an Experimental Introduction; Taylor & Francis: London, 1993.

17 M. Clemente-León, E. Coronado, C. J. Gómez-García and A. Soriano-Portillo. *Inorg. Chem.* 2006, **45**, 5653.

18 J. Nishijo, K. Judai, S. Numao and N. Nishi. *Inorg. Chem.* 2009, **48**, 9402.

19 W. W. Shum, Y. Liao and J. S. Miller, *J. Phys. Chem. A.* 2004,**108**, 7460.

Table 1. Crystallographic data and structure refinement details for complexes **1** and **2**

Complex	**1**	**2**
Empirical formula	$C_4H_{18}KMn_2Ru_2Br_2O_{21}$	$C_2H_{14}MnRuBrO_{13}$
M	913.10	482.04
Crystal system	Tetragonal	Monoclinic
Space group	$P4_2/mbc$	$C2/m$
a [Å]	11.9037(17)	17.221(2)
b [Å]	11.9037(17)	15.9645(18)
c [Å]	16.046(3)	11.0234(13)
α [°]	90	90
β [°]	90	114.308(2)
γ [°]	90	90
V [Å^3]	2273.7(6)	2761.8(6)
Z	8	8
ρ_{calcd} [g·cm^{-3}]	2.679	2.251
μ [mm^{-1}]	6.180	4.955
F(000)	1751	1760
GOF on F^2	1.069	1.113
Reflections collected	17439	6735
$R_{(int)}$	0.097	0.033
R_1, wR_2 [$I>2\sigma(I)$][a]	0.0470, 0.1138	0.0408, 0.1278
$(\Delta\rho)_{max}$, $(\Delta\rho)_{min}$ [e/Å^3]	1.103, -0.568	1.691, -1.078

[a] $R_1 = \Sigma||F_o| - |F_c||/\Sigma|F_o|$; $wR_2 = [\Sigma w(F_o^2 - F_c^2)^2/\Sigma w(F_o^2)^2]^{1/2}$

Table 2. Selected bond lengths (Å) of complexes **1** and **2**

		1	
Ru(1)–Ru(1A)	2.2780(13)	Mn(1)–O(3)	2.170(5)
Ru(1)–Br(1)	2.7234(16)	Mn(1)–O(4)	2.240(6)
Ru(1)–O(1)	2.035(5)	Mn(1)–O(5)	2.187(6)
Ru(1)–O(2A)	2.029(5)		
		2	
Ru(1)–Ru(1A)	2.2693(13)	Ru(2)–Ru(2B)	2.2731(10)
Ru(1)–Br(1)	2.7267(17)	Ru(2)–Br(2)	2.6948(13)
Ru(1)–O(1)	2.027(5)	Ru(2)–O(4)	2.026(5)
Ru(1)–O(3)	2.015(5)	Ru(2)–O(6)	2.021(5)
Mn(1)–O(2)	2.160(6)	Mn(1)–O(8)	2.259(5)
Mn(1)–O(5)	2.153(5)	Mn(1)–O(9)	2.203(5)
Mn(1)–O(7)	2.146(6)	Mn(1)–O(10)	2.193(7)

Symmetry codes: **1:** A, -x + 1, -y + 2, z. **2:** A, 1-x, -y, 2-z; B, -x, -y, 1-z.

Table 3. Structures and magnetic parameters for the series of Mn-$Ru_2(CO_3)_4^{3-}$ carbonate assembles.

Complex	Dimension	MnO_6 linking mode	$T_C(\chi')$	$T_C(\chi'')$
$K[\{Mn(H_2O)_4\}_2Ru_2(CO_3)_4Br_2]\cdot H_2O$	1D this work	*cis*	2.6K; 4.9K	2.7K; 5.2K
$H[\{Mn(H_2O)_4\}_2Ru_2(CO_3)_4Br_2]\cdot 6H_2O$	1D this work	*cis*	2.8K	none
$K[Mn(H_2O)_5Ru_2(CO_3)_4]\cdot 5H_2O$	2D[11g]	monosubstituted	3.8K	3.8K
$KMn(H_2O)_6[Mn(H_2O)_2Ru_2(CO_3)_4Cl_2]\cdot 4H_2O$	2D[11d]	cross	5.0K	5.2K
$K[Mn(H_2O)_4Ru_2(CO_3)_4]\cdot H_2O$	3D[7b,c]	*cis*	4.8K	5.4K
$Mn_4(H_2O)_{16}H[Ru_2(CO_3)_4]_2[Ru_2(CO_3)_4(H_2O)_2]\cdot 11H_2O$	3D[11a]	*cis* and *trans*	2.9K	3.2K

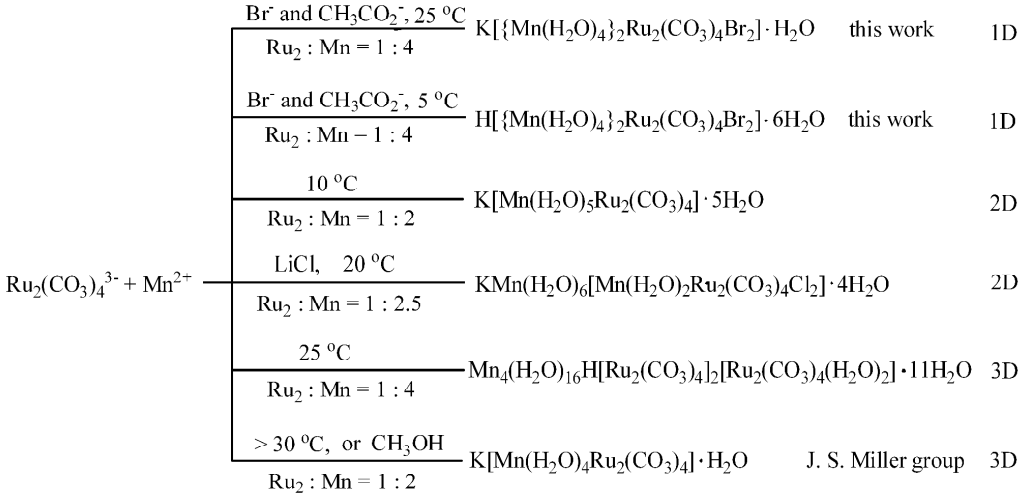

Scheme 1. The self-assembling of $Ru_2(CO_3)_4^{3-}$ and Mn^{2+} in aqueous solution reported by J. S. Miller and our research groups.

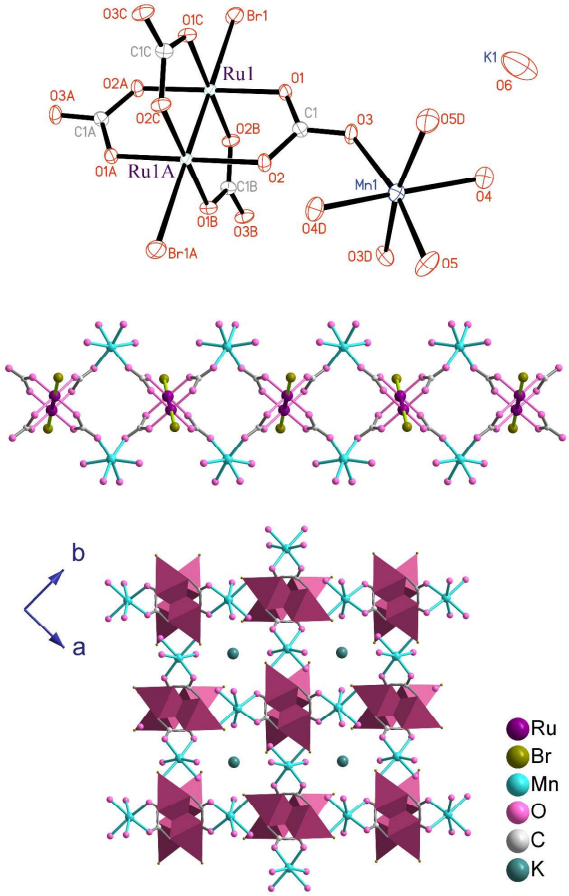

Fig 1. Top: ORTEP representation (30% thermal probability ellipsoids) of the structure of **1.** Middle: The infinite *α*-chain structure of complex **1**. Bottom**:** Packing diagram of complex 1 running along the *c* axis (purple Ru in an elongating octahedral environment). Symmetry codes: A, -x + 1, -y + 2, z; B, -x + 1, -y + 2, -z; C, x, y, -z; D, -y + 3/2, -x + 3/2, -z + 1/2.

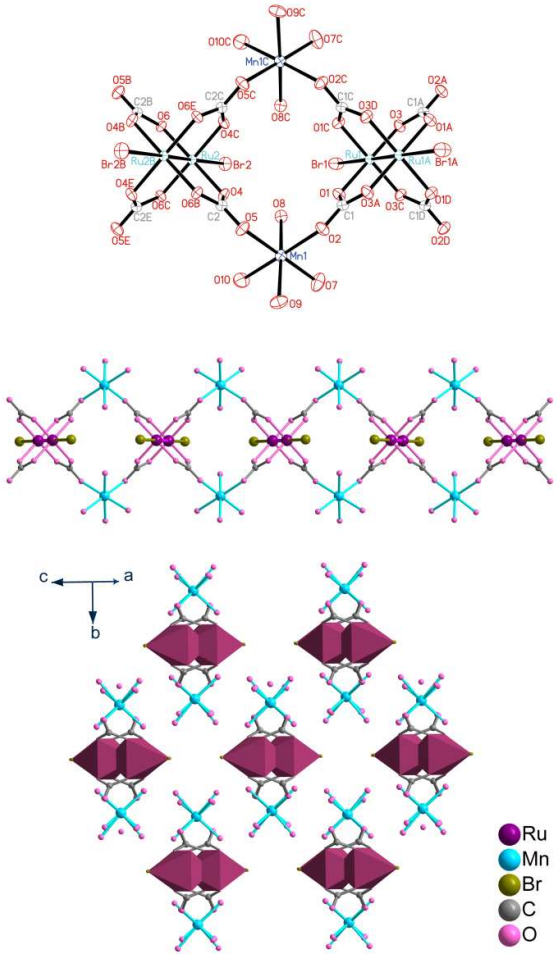

Fig 2. Top: ORTEP representation (30% thermal probability ellipsoids) of the structure of **2.** Middle: The infinite *β*-chain structure of complex **2**. Bottom**:** Packing diagram of complex 2 running along the chain (purple Ru in an elongating octahedral environment). Symmetry codes: A, 1-x, y, 2-z; B, -x, y, 1-z; C, x, -y, z.

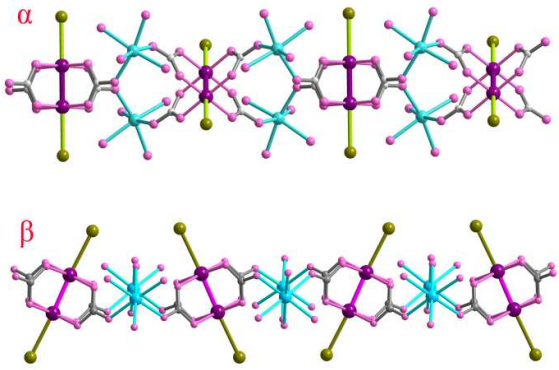

Fig 3. The isomeric α-(twisted) and β-(zigzag) double chains of $\{[Mn(H_2O)_4]_2Ru_2(CO_3)_4Br_2\}_n^{n-}$ in complexes **1** and **2**, respectively, from the side view.

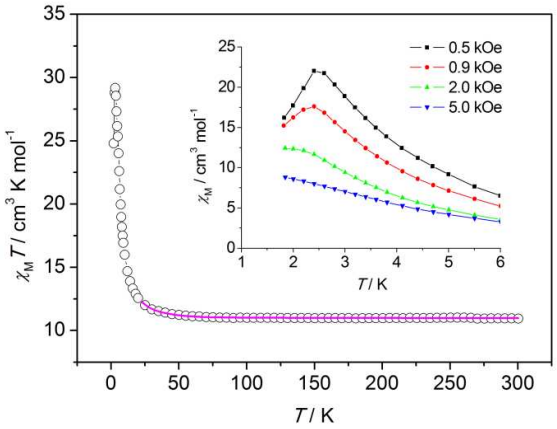

Fig 4. $\chi_M T$ and χ_M vs T plots for **1.** Inset: χ_M in an applied field of 0.5, 0.9, 2.0, and 5.0 kOe for **1.**

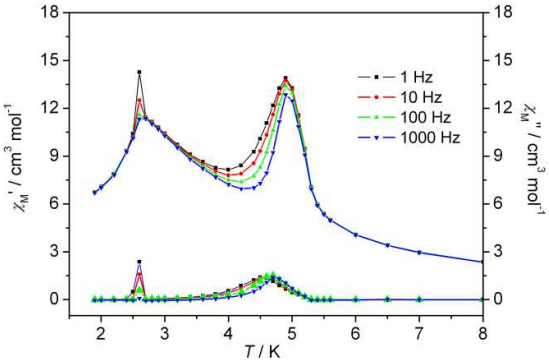

Fig 5. χ_M' and χ_M" vs T plots for **1.**

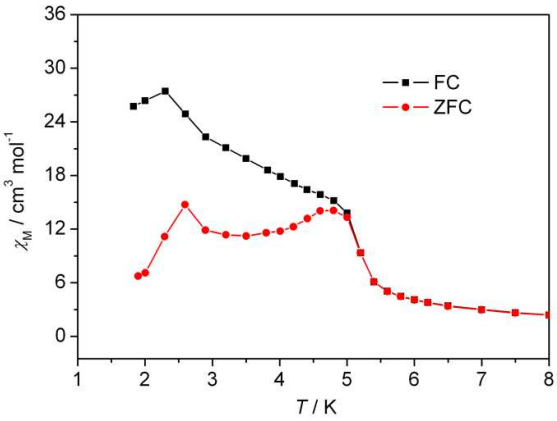

Fig 6. FC and ZFC vs T plots for **1.**

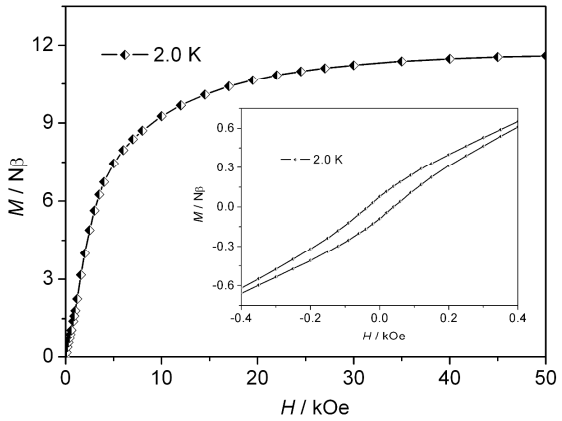

Fig 7. Magnetization *M* in Nβ units vs *H* plot for complex **1.**

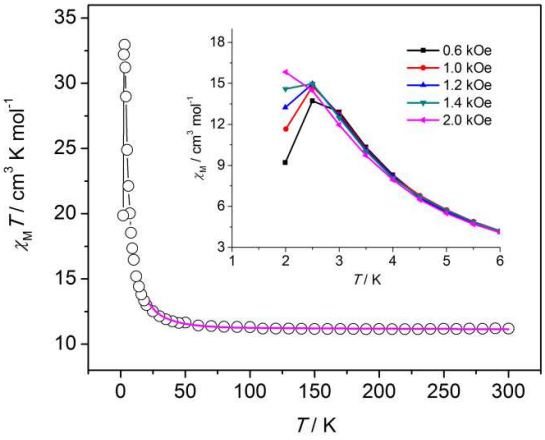

Fig 8. $\chi_M T$ and χ_M vs *T* plots for **2.** Inset: χ_M in an applied field of 0.6, 1.0, 1.2, 1.4, and 2.0 kOe for **2.**

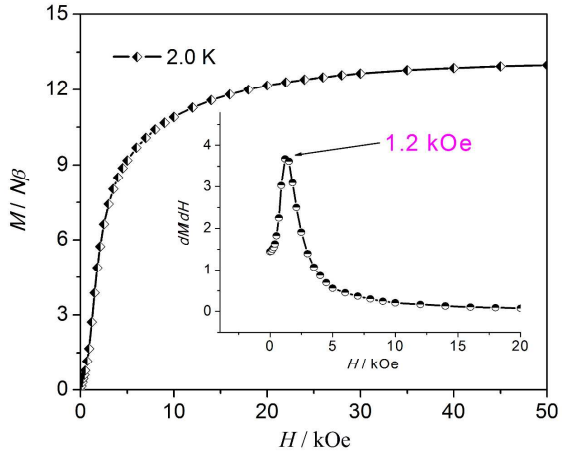

Fig 9. Magnetization *M* in Nβ units vs *H* plot for complex **2**. Inset: the critical field determined by the d*M*/d*H* curve.

Isomeric (twisted and zigzag) double-chain $\{[Mn(H_2O)_4]_2Ru_2(CO_3)_4Br_2\}_n^{n-}$ complexes show two-step magnetism ordering (5.0 K and 2.6 K) and metamagnetism behavior (1.2 kOe).